Available online at www.sciencedirect.com

SciVerse ScienceDirect

Structural Integrity Procedia 00 (2016) 000–000

Structural Integrity Procedia

www.elsevier.com/locate/procedia

21st European Conference on Fracture, ECF21, 20-24 June 2016, Catania, Italy

Computational Model for Delamination Growth at SMA-GFRP Interface of Hybrid Composite

A. Lo Conte[a,*], C.A. Biffi[b], A. Tuissi[b], A. Ali[a]

[a]*Politecnico di Milano, Department of Mechanical Engineering, Via G. La Masa 1, Milano 20156, Italy.*
[b]*National Research Council CNR, Institute for Energetics and Interphases, Corso Promessi Sposi, 29, Lecco 23900, Italy.*

Abstract

A cohesive model of the new interface of the *CuZnAl* SMA/GFRP hybrid composite is proposed and the interfacial delamination under Mode II loading conditions, between plain *CuZnAl* SMA sheet insert and GFRP matrix, as well as between *CuZnAl* SMA sheet insert having elliptical hole pattern and GFRP matrix, are studied in detail.
The results of the pull-out tests with plain sheet insert are used to calculate the interfacial parameters of the hybrid composite. With these parameters, the cohesive interaction and failure mechanism for hybrid composite with plain sheet, as well as with patterned sheet insert, is modelled. The efficacy of the laser patterned SMA sheet inserts to improve the overall interfacial strength in the new laminated SMA/GFRP hybrid composite for applications, such as light weight and high damping material under dynamic loads, is validated.

Peer-review under responsibility of the Scientific Committee of ECF21.

Keywords: Hybrid composite, Delamination, Finite element analysis, Cohesive interface;

1. Introduction

Since Shape Memory Alloy (SMA) hybrid composites were first proposed, these composites have attracted great attention for the improvement of creep and fatigue properties, strength and damping capacity, large recoverable strain and recovery stress, and also to control the shape and vibration response properties, natively with "multi-functionality" or adaptive properties. A variety of SMA hybrid composites have been designed, with SMA elements being either the matrix or the reinforcement (Zhang and Zhao (2007)). Among these materials, the SMA/Glass Fibre Reinforced Polymer (GFRP) hybrid composite with SMA embedded in the bulk GFRP, is especially very important due to the enormous potential to be used in real-life engineering environment, thereby exploiting its light weight, stiffness and damping properties (Ni et al. (2007)).

In Bocciolone et al. (2013), a new design interface of SMA/GFRP hybrid composite, in the shape of thin beams or plates, was proposed. The objective of this design was to improve the structural damping of the GFRP structure for

* Corresponding author. Tel.: +39-02-2399-8223 ; fax: +39-02-2399-8202.
E-mail address: antonietta.loconte@polimi.it

Peer-review under responsibility of the Scientific Committee of ECF21.

applications at room temperature, without changing its stiffness and weight significantly, also focusing on manufacturability and cost effectiveness for industrial applications. Thin sheets of $Cu_{66}Al_{24}Zn_{10}$, were selected as inserts in a $[45/+45]_n$ layered GFRP host composite. The thin SMA sheets were laser patterned with the aim of improving adhesive strength between the host laminated composite and the inserts. In Bocciolone et al. (2013), the strength of the interface between GFRP and *CuZnAl* SMA layer of the hybrid composite was studied by means of pull-out tests on *CuZnAl* SMA sheets (both plain and laser patterned with elliptical holes) embedded in layered GFRP host composite. The effect of the hole pattern of the SMA sheet on the load transfer capacity of the interface was investigated. The results showed that the increase in the overall load transferability and the interface strength, due to the presence of holes in the insert, is far greater than the decrease due to the reduction in the area of the contact (responsible for load transfer by the shear stress) between the insert and the matrix. While the pull-out test on the hybrid composite with plain SMA sheet insert showed complete delamination, the hybrid composite with SMA sheet insert having elliptical laser patterned holes showed only an initiation of the delamination in a very thin band at the edge of the interface area followed by the failure of the insert. A plausible reason is that, if there are holes in the laminate inserts, the load is transferred between the bulk matrix and the insert by the shear stress at the interface among the parallel faces and also by the normal stress between the insert and the matrix inside the holes, when the composite is loaded in tension.

In this paper, a cohesive model of the new interface of the *CuZnAl* SMA/GFRP hybrid composite is proposed and the interfacial behaviour is studied in detail. The aim of the work is the validation of the efficacy of the laser patterned SMA sheet inserts to improve the overall interfacial strength in the new laminated SMA hybrid composite for applications, such as light weight and high damping material under dynamic loads. The validation is based on finite element analysis run with *Abaqus* code.

Nomenclature

σ	stress
δ	displacement jump
K	contact/*penalty*/interfacial stiffness
K_{nn}	contact/*penalty*/interfacial stiffness in normal direction
K_{ss}	contact/*penalty*/interfacial stiffness in shear direction 1
K_{tt}	contact/*penalty*/interfacial stiffness in shear direction 2
τ_{max}	maximum contact stress in first or second shear direction
F_{max}	maximum force for complete pull-out of SMA sheet
$A_{cont.}$	total area of interface/contact between GFRP & SMA
δ_i	displacement jump corresponding to damage initiation
δ_f	displacement jump at the complete failure of the interfacial cohesion
σ_n^o	maximum normal stress
τ_s^o	maximum shear stress in shear direction 1
τ_t^o	maximum shear stress in shear direction 2
D	scalar damage variable

2. Cohesive damage model

Delamination can be analysed by using *cohesive damage models* and *fracture mechanics*. A cohesive damage model implements interfacial constitutive laws defined in terms of damage variable and a damage evolution law. In the fracture mechanics approach, the propagation of an existing delamination is analysed by comparing the amount of energy release rate with the fracture toughness of the interface. When mixed mode conditions are involved, the decomposition into mode I, mode II, and mode III components becomes necessary due to the mixed-mode dependency of interface toughness (Hutchinson and Suo (1992)). A number of fracture mechanics-based models have been put forward in the literature to study delamination, including three-dimensional models and simplified beam-like models. The *Cohesive Zone Model* (CZM) for the numerical simulation of delamination is based on the concept of cohesive

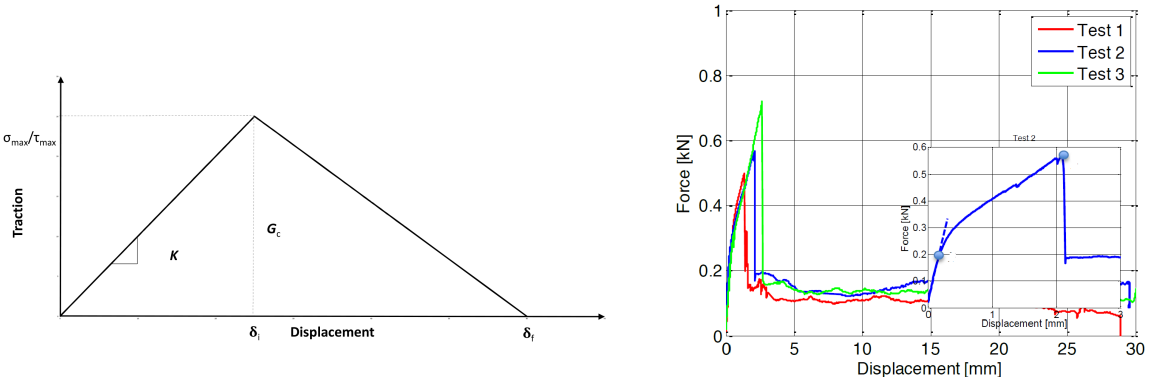

(a) (b)

Fig. 1: a) Bilinear traction separation response for cohesive zone model. b) Results of pull-out test of specimens with plain SMA sheet.

crack model at the interface with the development of a cohesive damage zone along the front of the delamination where there are displacement and stress singularities due to both the material and the geometrical discontinuities (Zhao et al. (2014)). CZM is based on the supposition that the stress transfer capacity between the two separating faces of a delamination is not lost completely at damage initiation, but rather is a progressive event governed by progressive stiffness reduction of the interface between the two separating faces. This approach is capable of capturing the physics of the delamination failure and can be used in the numerical formulation of zero thickness cohesive interface elements for finite elements analysis. The CZM element with zero thickness is implemented in *Abaqus* code through interaction with cohesive behaviour (Coelho (2016)). The element stiffness matrix requires the stiffness K of the interface material (*penalty* stiffness), but the element stiffness matrix is not formulated as usual by integration over the volume of the element because the initial volume of the element is zero. Since the initial thickness of the CZM element is zero, the deformation state of the CZM element can not be described by the classical definition of strain. Instead, the measure of the deformation becomes the separation (slip) δ between the faces connected through the cohesive surface, and this makes possible the use of the (σ - δ) traction-separation equation instead of the classical engineering (σ - ϵ) equation. Although the cohesive damage models cannot be referred to as non-local damage models (M. Jiràsek and Z.P. Bažant (2002)), they allow a mesh-independent representation of material softening, provided that the mesh is refined sufficiently.

3. Formulation of the Cohesive Zone Model

CZM gives the traction-separation relation for the interface. The traction across the interface increases and reaches a peak value, then decreases and eventually ceases, allowing complete decohesion. In the FE models discussed in the following sections, a bilinear cohesive law is implemented which reduces the artificial compliance inherent in the intrinsic CZM (Fig.1a). The relative displacement across the interface is denoted as δ. Mode II delamination failure caused by shear stress between the GFRP matrix and *CuZnAl* sheet insert is representative of the in-service condition of the investigated interface in a vibrating slender beam or thin plate. While normal stresses are negligible, as no constraint in the normal direction is present. According to this loading condition, reproduced in the pull-out tests, a pure shear slip, by itself, does not induce cohesive forces in the normal direction, and pure normal separation does not induce cohesive forces in the shear direction 1 or 2 (uncoupled behaviour). The elastic traction-separation behaviour can be represented as

$$\begin{bmatrix} \sigma_n \\ \tau_s \\ \tau_t \end{bmatrix} = \begin{bmatrix} K_{nn} & K_{ns} & K_{nt} \\ K_{ns} & K_{ss} & K_{st} \\ K_{nt} & K_{st} & K_{tt} \end{bmatrix} \begin{bmatrix} \delta_n \\ \delta_s \\ \delta_t \end{bmatrix} \tag{1}$$

where n denotes normal direction, *s* denotes shear direction 1 (mode II) and *t* denotes shear direction 2 (mode III). A simplest specification of cohesive behaviour, which generates contact penalties that enforce the cohesive constraint in both normal and tangential directions, can be adopted. The terms K_{nn}, K_{ss} and K_{tt} of eq. (1), are defined and calculated, and it is assumed $K_{ns} = K_{nt} = K_{st} = K_{sn} = K_{tn} = K_{ts} = 0$. The interface stiffness or contact stiffness or *penalty* stiffness (K_{ss} and K_{tt}) is calculated by considering the limiting value of maximum contact shear stress for the interface and the displacement jump corresponding to this value, obtained from pull-out tests with plain SMA insert (Fig.1b). The maximum shear stress for the interface can be calculated by the maximum force in the pull-out test along with the area of contact between the GFRP bulk and the SMA layers. The table 1 shows the values of maximum shear stress for the contact and *penalty* stiffness along shear direction, as obtained for the the three pull-out tests with plain sheets.

Table 1: Maximum load, maximum contact shear stress and *penalty* stiffness in mode II for pull-out tests with plain sheets.

	Test 1	Test 2	Test 3	Average
Force, F(N)	500	567	719	595
Max. shear $\tau_{max}(N/m^2)$	416666	472500	599166	496111
Penalty stiffness K_{ss} (N/m^3)	3.015×10^8	2.251×10^8	2.241×10^8	2.502×10^8

The degradation and failure of the interfacial cohesion between two surfaces can be represented by a damage model. The main concepts of this model are, a *Damage initiation criterion* and a *Damage evolution law*. As represented in Fig.1a, the response of the interface upon the application of a force is linear up to a certain point when the *Damage initiation criterion* is met. This is represented by the maximum stresses in mode I, II and III, respectively, which the interface is able to sustain. The *Damage initiation criterion* refers to the starting of the degradation of the cohesive behaviour at a contact pair. After this point the degradation of the interface cohesion starts. This degradation can be modelled by a *Damage evolution law*. The degradation starts when the contact stress and/or contact separation (depending upon the choice of the criterion) reaches a limit value. Here, maximum stress criterion is considered as damage initiation criterion. The damage is assumed to start as soon as the maximum contact stress(interfacial stress) ratio reaches a value of unity. This damage initiation criterion can be represented as

$$max\left\{\frac{\langle\sigma_n\rangle}{\sigma_n^o}, \frac{\tau_s}{\tau_s^o}, \frac{\tau_t}{\tau_t^o}\right\} = 1 \tag{2}$$

where the maximum shear stress for the interface are the ones reported in the table 1.

As soon as the damage initiation criterion is fulfilled, the rate at which the interfacial *penalty* stiffness is degraded is described by the *Damage evolution law*. Given the hypothesis of uncoupled normal and tangential failure modes, the overall damage at any contact pair of the cohesive surfaces can be represented by a scalar damage variable 'D'. Initially, it has the value of 0. As soon as the damage initiation criterion is reached, D evolves from 0 to 1. Fracture toughness or critical energy release rate (the energy dissipated during the damage, G_c) can be used to define the damage evolution. The value of G_c is equal of the area under the traction-separation curve. This parameter, along with maximum contact stress and *penalty* stiffness, defines the evolution of the damage in this case. For the linear softening law, the evolution of the damage variable 'D' can be represented by the following expression:

$$D = \frac{\delta_f(\delta_{max} - \delta_i)}{\delta_{max}(\delta_f - \delta_i)} \tag{3}$$

where $\delta_f = 2G_c/\tau_{max}$(or σ_{max}). According to the bilinear constitutive law shown in Fig.1a (in absolute terms), which presents linear elastic and linear softening behaviour, the critical energy release rate may be calculated as $G_{II,IIIc} = 1/2\tau_{max}\delta_f$. On the basis of the calculated values for each test, an approximate value was selected for all the FE models for the simulation. These parameters will be used to model cohesive interaction for hybrid composite with plain SMA sheet, as well as, with patterned SMA sheet.

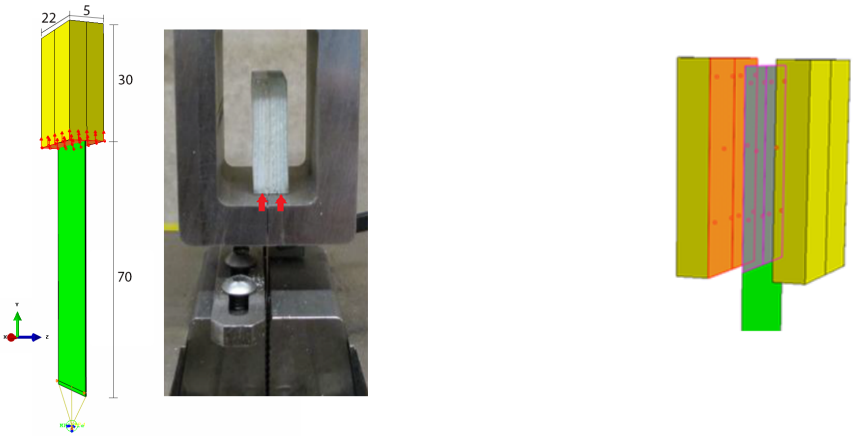

(a) (b)

Fig. 2: FE model for simulation of pull-out test with plain SMA insert. (a) Applied load, fixed boundary condition and MPC, along with loading condition in experimental pull-out test, (b) Surfaces for cohesive interaction.

4. Mode II delamination

A Finite Element (FE) model was set up for the simulation of the pull-out test of the hybrid composite specimen with plain SMA sheet insert, without any pattern. The FE model is shown in the Fig.2. The dimensions of the SMA sheets and of the GFRP block were the same of the pull-out tests (Fig.2a). The GFRP blocks were modelled as 3D solids while the SMA sheet was modelled as 3D shell. A reference point (*RP*)) was created to constrain the sheet. After checking for convergence, 1 mm 3D linear elements with *reduced integration* (C3D8R) were used for the GFRP blocks and 1 mm linear shell elements with *reduced integration* (S4R) were used for the SMA sheet. The interface between GFRP blocks and the SMA sheet was modelled by using the cohesive surfaces/interactions between the GFRP blocks and both sides of the SMA sheet, Fig.2b. This was done by defining surface-to-surface contact with interaction properties defined by *Cohesive behaviour* and *Damage* defined in the previous section. The GFRP was described as homogeneous material with appropriate modulus with ±45° lay up, E=16.5 GPa, and Poisson's coefficient $\nu = 0.35$. The behaviour of the *CuZnAl* alloy sheet, with 0.3mm thickness, was described with the experimental stress-strain curve (Bocciolone et al. (2012)). The displacement boundary condition along *Y* direction was applied on the lower face of the GFRP blocks Fig.2a, along with indication of the location for the force application in experimental set-up.

Two *Nonlinear Static* analysis steps were defined. The first analysis step was defined to establish a stable contact between the *master* and *slave* nodes of the contacting surfaces of cohesive node pairs. In the second analysis step, displacement boundary condition is applied and the response of the model was obtained by monitoring the reaction force and the damage on the cohesive interface. The interfacial stiffness estimated by the curve of the experimental test results shown in Fig.1 for test 1, 2 and 3, and reported in table 1, were used as initial stiffness values.

The first important result is that the deformed model results corresponding to the maximum reaction force, for the three pull-out tests, are the same as the experimental results (with a very little error). Also, complete delamination and slip condition can be observed as in the experimental cases.

For the same tests, a sensitivity analysis of the displacement jump versus tangential stiffness was performed. The results are reported in Fig.3a for test 1. The value of the tangential stiffness for which the exact displacement corresponding to the maximum force was obtained, is reported in table 2 and compared with the experimental values, for test 1, 2, and 3.

No data was available related to the *penalty* stiffness and damage values for the normal direction. A value of zero for *penalty* stiffness in the normal direction is suggested in *Abaqus* code documentation, when mode I is not relevant or there is no force in the normal direction, but it results in convergence difficulties. So, it was obtained by running a series to simulations by carefully optimizing the runtime and a sound contact between the interacting surfaces. Finally, a value of $1 \times 10^{12}\ N/m^3$ was selected.

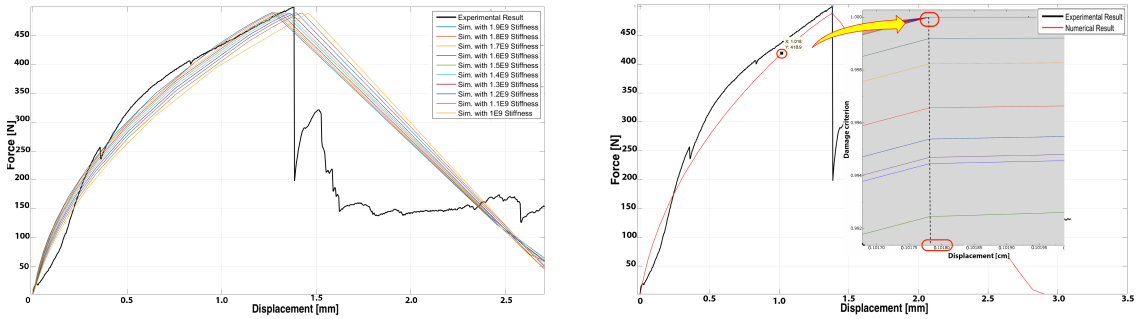

(a) (b)

Fig. 3: (a) Numerical results of analysis for stiffness adjustment of pull-out Tets1. (b) Numerical calculation of minimum force for damage initiation, for pull-out Test 1.

A very important result from the numerical simulation is the calculation of the minimum force required for the damage initiation (F_d). It could not be determined from the experimental results because of the characteristic non-linear behaviour of the SMA material. To determine the minimum force for damage initiation, the damage initiation criterion curve was plotted against displacement for all the contacting node pairs (Fig.3b). The displacement jump, when damage initiation criterion is satisfied for the very first contact node pair, was traced on the force displacement curve to get the value of F_d. The maximum force and corresponding displacement jump for the pull-out tests with plain SMA sheet insert are reported in table 3.

Table 2: *Penalty*/tangential stiffness calculated from pull-out tests and corrected values for simulation.

	Test 1	Test 2	Test 3	Average
Calculated(N/m^3)	3.015×10^8	2.251×10^8	2.241×10^8	2.502×10^8
Simulated(N/m^3)	1.2×10^9	6.0×10^8	1.4×10^9	1.07×10^9

Table 3: Experimental vs numerical results for maximum force and corresponding displacement jump.

Test	Maximum Force, F_{max} (N)			Displacement at F_{max}, δ_i (mm)		
	Experimental	Numerical	Error	Experimental	Numerical	Error
1	500	488.0	2.40%	1.382	1.380	0.14%
2	567	553.4	2.40%	1.382	1.380	0.14%
3	719	702.7	2.27%	2.673	2.681	0.30%

5. Modelling of interface with patterned *CuZnAl* SMA sheet

A Finite Element (FE) model was set up for the simulation of the pull-out test of the hybrid composite specimen with insert having elliptical holes pattern. This model takes into account the *CuZnAl* SMA-GFRP interaction along the parallel faces, as in the case of plain insert, and also the interaction of GFRP and SMA material on the inner surface of the elliptical holes. The exploded view of the of the model is shown in Fig.4a. For the purpose of mesh refinement and reducing simulation time, the GFRP blocks were divided into two parts, one larger part with coarser mesh and other smaller part with finer mesh contacting the SMA sheet. These two pieces of the same part were joined by using *Tie* constraint. The parts shown in green colour were assigned SMA while those shown in yellow colour were assigned GFRP material. The overall dimensions of the model were same as the previous model with plain SMA sheet insert. The dimensions of the elliptical holes in the sheet and elliptical GFRP pieces were same and are shown in Fig.4b.

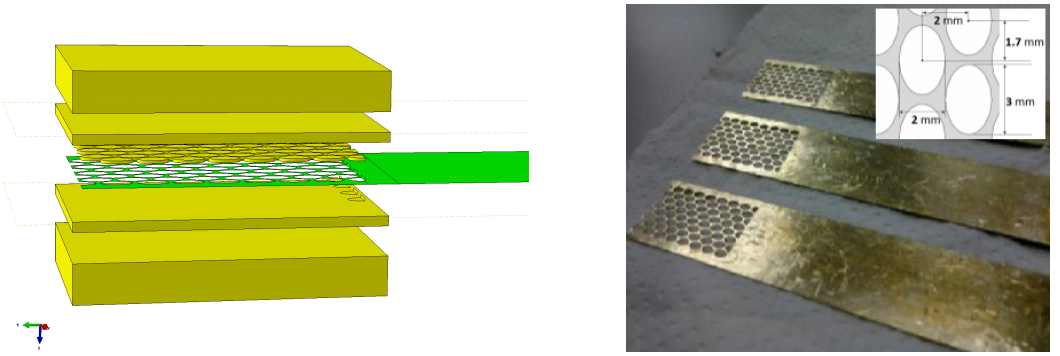

(a) (b)

Fig. 4: (a) Exploded model of the Interface with patterned *CuZnAl* SMA insert. (b) Sheets with elliptical hole pattern and geometry of the pattern.

Mesh sizing was different from what was chosen for the FE model with plain SMA sheet. This was contributed to the presence of the elliptical holes, thin SMA strands, overall more parts in the assembly & their interactions. Mesh size of 0.2 mm was chosen around the elliptical holes of SMA sheet, for GFRP elliptical & semi-elliptical parts and shell strips. For all the parts with any kind of interaction, care was taken to have mesh refinement on *Slave* surface and if the mesh density was same on both *Master* and *Slave* surfaces, *Slave* surface was chosen to be the one with softer underlying material. Mesh size of 0.4 mm and 1 mm was chosen for GFRP blocks. The part of SMA sheet away from elliptical holes was meshed with 0.8 mm elements. The element type for all shell parts was S4R, while for 3D solid parts, C3D8R elements were used.

The interface between the GFRP blocks and the SMA sheet faces was modelled by using the cohesive surfaces/interactions. The values of the parameters like *Cohesive behaviour* and *Damage* were the average of the parameters used for different tests in the previous case of plain SMA sheet. A contact interaction was created for the elliptical GFRP parts and the SMA sheets holes to prevent penetration. For this purpose, the *Normal behaviour* was defined by *Hard contact*, while *Tangential behaviour* was defined by using *penalty* friction formulation. This was done in order to compensate for the curing induced residual stresses that were present between the GFRP and SMA material because of their significantly different coefficients of thermal expansion.

Constraints of the reference point and displacement boundary condition were defined in a manner similar to what was explained in previous section and illustrated in Fig.2a. Two analysis steps were created for this model, exactly as before and similar output requests were created but smaller initial and minimum time increments were used. The shell semi-elliptical GFRP pieces coupled to the solid GFRP semi-elliptical pieces and small shell strips with GFRP and SMA properties, were used to optimise convergence and solution time without any loss of accuracy.

The comparison between the experimental test and numerical simulation of the failed SMA sheet is shown in Fig.5a. In this case, the mechanism of failure was different from the failure/pull-out of the specimen with plain SMA sheet insert, as seen in the experimental test, and from the geometry and condition of the failed specimen.

The main point to discuss here is that, even after the SMA sheet had failed at the thin strands, there was no delamination or failure of cohesive interaction between the patterned SMA insert and the GFRP (except along a thin band near the failure region of the SMA strands). It was observed in the *Damage criterion* plot that the damage initiation criterion is very far from being fulfilled (only 0.025 out of 1) and there was no interface damage. Also, the slope of the lines in the *Damage criterion* plot was approaching zero after some displacement, which suggested that the interface was unlikely to be damaged upon further loading. This result is completely in-line with the experimental results and with the requirements of an improved interfacial strength between the host GFRP and the *CuZnAl* SMA insert. The Fig.5b shows the force-displacement curve obtained as the result of numerical simulation and experimental pull-out test on hybrid composite specimen with patterned SMA sheet insert. The simulation was stopped when the maximum strain in the SMA sheet reached the strain value at the fracture, derived from the experimental tests. It is to be noted that the location of the maximum deformation in experimental results, as well as, the numerical results is exactly the same.

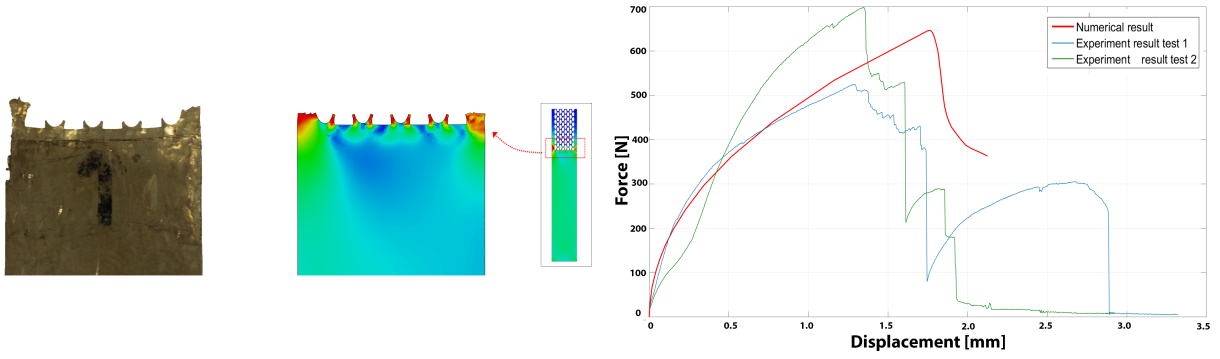

(a) (b)

Fig. 5: (a) Damage initiation criterion plot for all the contact node pairs. (b) Force-displacement curve for experimental and numerical results with patterned SMA.

6. Conclusions

A cohesive model of the new interface of the *CuZnAl* SMA/GFRP hybrid composite has been proposed and the interfacial delamination under Mode II loading conditions, between plain *CuZnAl* SMA sheet insert and GFRP matrix, as well as, between *CuZnAl* SMA sheet insert having elliptical hole pattern and GFRP matrix, has been investigated. The failure mechanism of the interface with elliptical holes pattern in the pull-out tests has been accurately simulated and, in agreement with the results from the experimental tests, it has been shown that upon loading, the interface between the patterned SMA sheet and the GFRP was intact without damage and the failure occurred due to the material failure. It has been assessed that the presence of curing stresses, between SMA sheets and epoxy material inside the holes, account for the improved overall interfacial strength between the *CuZnAl* SMA insert and the GFRP matrix. On the basis of these results, the effectiveness and efficacy of the laser patterned SMA sheet insert to improve the overall interfacial strength in the new laminated SMA/GFRP hybrid composite for applications, such as light weight and high damping material under dynamic loads, has been validated.

References

Zhang Y., Zhao Y.-P. , A study of composite beam with shape memory alloy arbitrarily embedded under thermal and mechanical loadings, in *Matrials and design*, Vol. 28.

Ni Q.Q., xin Zhang R., Natsuki T., Iwamoto M., Stiffness and vibration characteristics of SMA/ER3 composites with shape memory alloy short fibers, in *Composite Structures*, Vol. 79.

Bocciolone M., Carnevale M., Collina A., Lecis N., Lo Conte A., Previtali B., Biffi C.A., Bassani P., Tuissi A., Strength of SMA/GFRP interface in a new designed railway collector, 6th Conference on Smart Structures and Materials, Torino 24-26 June 2013, E. Carrera, F. Miglioretti,and M. Petrolo (Editors), www.smart2013.com.

S. Arnaboldi, P. Bassani, C.A. Biffi, A. Tuissi, M. Carnevale, N. Lecis, A. Lo Conte, B. Previtali, Strength of SMA/GFRP interface in a new designed railway collector, in *Conference on Smart Structures and Materials*.

J. W. Hutchinson, Z. Suo, Mixed mode cracking in layered materials, in *Advances in Applied Mechanics*, Vol. 29, pp. 63-191.

Libin Zhao, Yu Gong, Jianyu Zhang, Yuli Chen, Binjun Fei, Simulation of delamination growth in multidirectional laminates under mode I/II loadings using cohesive elements, in *Composite Structures*, Vol. 116, pp. 509522.

Ana M. Girão Coelho, Finite element guidelines for simulation of delamination dominated failures in composite materials validated by case studies, in *Archives of Computational Methods in Engineering*, Vol. 2, pp. 363-388.

M. Jiràsek and Z.P. Bažant, Nonlocal integral formulations of plasticity and damage: survey of progress, in *Journal of Engineering Mechanics*, Vol. 128, pp. 1119-1149.

M. Bocciolone, M. Carnevale, A. Collina, N. Lecis, A. Lo Conte, B. Previtali, C.A. Biffi, P. Bassani, A. Tuissi, N. Lecis, Design for Damping of a Railway Collector based on the Application of Shape memory Alloy, in *Smart Material Research*, Vol. 212, Art. ID 797319.

Paul W. Harper, Stephen R. Hallet, Cohesive zone length in numerical simulation of composite delamination, in *Engineering Fracture Mechanics*, Vol. 75, pp. 4774-4792.